Chemical Physics 555 (2022) 111455

Contents lists available at ScienceDirect

Chemical Physics

journal homepage: www.elsevier.com/locate/chemphys

Unraveling local structure of molten salt KF-KCl-KI via molecular dynamics simulation

Alexander Y. Galashev *, Ksenia A. Ivanichkina

Institute of High-Temperature Electrochemistry, Ural Branch, Russian Academy of Sciences, 20 Akademicheskaya Str., Ekaterinburg 620990, Russia
Ural Federal University Named After the First President of Russia B.N. Yeltsin, 19 Mira Str., Ekaterinburg 620002, Russia

ARTICLE INFO

Keywords:
Ions
Molecular dynamics
Molten salt
Structure
Voronoi polyhedra

ABSTRACT

The detailed structure and kinetic properties of the KF-KCl-KI salt melts were studied in the work. This ternary system is widely used to produce high-purity silicon by electrodeposition. The melt was at the temperature of 1000 K, the values of the diffusion coefficients of ions were predominantly arranged in a sequence determined by the ratio of inverse atomic masses. The radial distribution function and structural factor for melt ions were obtained. The structure of each subsystem of like ions is characterized by the prevalence of rotational symmetry of the 5th order. In the case of the I- ion subsystem, asymmetry appears in the distributions of Voronoi polyhedra both in topological and metric features. The angular distributions determined by the method of statistical geometry for ions of all types have a specific dome-like shape and indicate that the arrangement of three ions on the same line is an extremely rare event.

1. Introduction

Molten salts are widely used as electrolytes in the batteries, as well as a media for production of high-purity substances (precipitates), including thin films [1]. The electrical conductivity of the electrolyte is closely related to the structure of the melt and it is considered to be one of the most important properties [1,2,3]. An ionic association, which manifests itself, for example, in ions pairing and clustering, can significantly change the electrical conductivity of the electrolyte [4,5,6]. An increase in temperature, as a rule, creates conditions for an increase in the ion velocity and, consequently, the electrical conductivity. However, an increase in temperature does not necessarily result in the increase in the electrical conductivity. The point is that the liquid expands with increasing temperature, and the counterions approach each other [7,8]. This in turn increases the energy barrier for jumping to the next adjacent location [7,9,10]. When this happens, the temperature dependence of the conductivity passes through a maximum [11,12].

In many cases, the high mobility of certain ions ensures their high partial conductivity [2,3,13]. As a rule, lithium ions have the highest mobility and, hence, the highest electrical conductivity in combined salt melts [13]. In addition, ionic complexes are not unlikely to be formed in the salt melts. Generally, a complex bond can be considered as an electrostatic interaction between donor and acceptor. In extreme cases, complexation can manifest itself both in the form of physical association and in the form of chemical complexation. The following experimental facts are known about the studied system. The introduction of a large amount of heavy salt (KI) into the composition of the melt leads to a decrease in its thermal conductivity [14,15]. Due to the complexation in the salt melt, its electrical conductivity changes with a significant deviation from additivity [16]. The complexation has a similar effect on the thermal conductivity [17]. The experimentally performed variation in the composition of the KF-KCl-KI salt melt showed that the molar volumes of the melts are close to those calculated by the additivity rule [18]. This means that the original salts are mixed without any visible chemical interaction. Thermal analysis of the cooling curves in combination with differential scanning calorimetry showed that the KF - KCl - KI system is characterized by the eutectic 25KF – 34KCl – 41KI (mol%) with a melting point of 750 K [19]. A correlation of viscosity and data from synchronous thermal analysis makes it possible to determine the mechanism of K_2SiF_6 decomposition in the $(KF\text{-}KCl)_{eut}$ - (10 mol%) K_2SiF_6 system [20]. The K_2SiF_6 decomposition results in the formation of KF and SiF_4. It was shown that at $T < 898$ K the melt had the form of suspension.

High-purity silicon wires and films can be obtained by Si deposition from the KF-KCl-K_2SiF_6 melt [21]. This electrolyte is less aggressive than the KF-KCl melt [22,23]. It is water-soluble and provides a stable supply

* Corresponding author.
E-mail address: galashev@ihte.uran.ru (A.Y. Galashev).

https://doi.org/10.1016/j.chemphys.2022.111455
Received 13 August 2021; Received in revised form 20 December 2021; Accepted 8 January 2022
Available online 12 January 2022

Table 1
Parameters of the BMH potential describing interactions in the KF-KCl-KI salt melt.

	B_{ij} (eV)	β_{ij} (Å)	σ_{ij} (Å)	Cij (eV×Å^6)	D_{ij} (eV×Å^8)	Ref.
K-K	0.2641	0.3003	2.926	15.19	−15.0	[25]
K-Cl	0.2113	0.3003	3.048	30.0	− 6.438	
Cl-Cl	0.1584	0.3003	3.170	11.576	− 13.69	
K-I	0.21098	0.355	3.37	12.135	−15.68	[26]
I-I	0.1592	0.355	3.814	11.5756	−13.691	
K-F	0.2113	0.338	3.1965	12.1358	−13.0689	[27]
F-F	0.1582	0.338	3.143	11.5756	−13.6911	
F-Cl	0.1583	0.3179	3.1565	11.5756	−13.6911	[28]
F-I	0.1587	0.3471	3.4785	11.5756	−13.6911	
Cl-I	0.1588	0.3279	3.492	11.5756	−13.6911	

of silicon during precipitation. Kim et al [1] reported that the electrodeposition of thin silicon films on substrates made of pyrolytic graphite and tungsten was performed using the KF-KCl (2: 1) – (75 mol%) KI melt containing 0.075 or 0.5 mol% of K_2SiF_6. Thin silicon films were obtained under galvanostatic conditions at 998 K. It is obvious that the structure of the melt used has a significant effect on the morphology and structure of the resulting deposit, i.e. silicon films. Diffusion-kinetic limitations observed during the growth of Si films are explained by an increase in the strength of the Si-F bond in the melt with a high KI content [1]. It is assumed that potassium iodide stabilizes the melt and has a favorable effect on the formation of silicon films.

Until now, the composition of the molten salt used for the deposition of silicon on a carbon substrate has been selected empirically. The impact of the melt components on the formation of a continuous and homogeneous Si film requires careful considerations. We assume that the computer simulation is the most effective way to solve this problem, because it allows us to determine the kinetic properties of each component of the molten salt and their detailed structure.

The purpose of this work is to study in detail the structure of the melt of the KF-KCl (2: 1) – (75 mol%) KI composition at a temperature of about 998 K, as well as to establish the possibility of the formation of associates in such systems and to investigate the correlation between the partial diffusion coefficients and the nearest environment of ions in the system.

2. Materials and methods

Certain requirements were imposed on the composition of the molten salt. In particular, we are engaged in the study of an oxygen-free combined salt melt. Oxygen-containing salts do not possess the required thermochemical stability at high temperatures. In addition, oxygen containing molten salt cannot be used if carbon materials such as a graphite electrode are used in the cell design. Oxygen released at high temperatures reacts quickly with available carbon.

To simulate the crystal and liquid phases of alkali halides, we used the pair potential Born-Mayer-Huggins (BMH) [24]

$$\Phi_{ij}(r) = Z_i Z_j \frac{e^2}{4\pi\varepsilon_0\varepsilon r} + B_{ij} exp\big(-[r-\sigma_{ij}]/\beta_{ij}\big) - \frac{C_{ij}}{r^6} - \frac{D_{ij}}{r^8} \quad (1)$$

where i and j can represent positive or negative ion, Zi and Zj are ± 1, in the case when the system is completely ionic and dipole–dipole and dipole-quadrupole terms are included; ε_0 and ε are the permittivity of the free space and the studied environment, respectively.

The parameters of the Born-Mayer-Huggins potential for the KF-KCl-KI molten salt determined in [25–28], are presented in Table 1. The energy calculated using this potential agrees very well with the Hartree-Fock energy. The use of more realistic models that directly take into account ion polarization is not always justified. A more careful consideration of the ion polarization creates significant problems associated with a useless extra cost of the calculation without noticeable benefit to the accuracy [29]. However, simulating aqueous solutions, the polarization should always be considered to eliminate incorrect results. It can be stated that an explicit consideration of polarization does not provide a more accurate description of the structure of simple alkali metal halides; however, the dynamics of such systems depends more strongly on the polarizability [30].

The initial configuration of the system under study was prepared in two stages. The first stage was aimed at the creation of a model of a completely melted superheated KF-KCl-KI system. The second stage of the preparatory operation was devoted to obtaining an equilibrium melt at an operating temperature of 1000 K. The simulation details of both stages are presented in Supplementary Material. At the first stage, KCl, KF, KI crystals with an FCC lattice were placed in a rectangular parallelepiped box. The minimum distance between ions of different types and between the ions and the walls of the box was 0.4 nm. The system consisted of 8992 ions, where 1728 ions represented KF (19.2 mol%), 864 ions represented KCl (9.6 mol%), and 6400 ions represented KI (71.2 mol%).

Periodic boundary conditions acted in three directions (x, y, z). The integration of Newton's equations of motion was carried out with a time step 1 fs. A geometric optimization was performed prior to molecular dynamics calculations. The geometric optimization ended when the system reached the minimum potential energy value. Then, in the NVT ensemble, the system was heated stepwise to 1750 K with a temperature step of 50 K for 3.5 ns. The transition of the system to a liquid state was controlled by the behavior of the potential energy, as well as by the form of the total and partial radial distribution functions.

The second stage of calculations was devoted to achieving the required melt density at 1000 K ($\rho \approx 2.27$ g / cm^3 [18]). The superheated melt was cooled stepwise from 1750 K to an operating temperature of 1000 K with a temperature step of 50 K in the NPT ensemble for 5 ns. It should be noted that the experimental temperature of the real electrolytic process ranges from 993 to 998 K and varies depending on the molar concentration of the components [21]. The change in the volume of the system, carried out during the implementation of calculations in the NPT ensemble, led to a change in the shape of the MD box, and it approached to the cube shape.

At this stage, the simulated melt reached the required density of 2.12 g / cm^3 and in further calculations, this density value remained unchanged. The experimentally obtained KF-KCL-75 mol% KI melt at 1000 K has a density of 2.27 g / cm^3, which is 6.6% higher than that obtained in the present model. The film was further deposited for 20 ns. Even in the ab initio molecular dynamics study of molten salts in an NPT ensemble, small errors in energy calculations led to a significant decrease in the density of the system. The system is considered to be in an equilibrium state if the values of energy remains unchanged within 2% over 10,000 time steps ($\Delta t = 0.5$ fs) [31]. Note that the duration of our resulting calculation exceeds the specified time interval by at least 4000 times. The thermostat relaxation time was $\tau_T = 40\Delta t$ and the barostat relaxation time was $\tau_P = 100\ \Delta t$ ($\Delta t = 1$ fs). Exactly the same values of the parameters τ_T and τ_P were used in [32].

Subsequent calculations were carried out with rigid impermeable side walls and the same upper wall of the MD cell and a graphite substrate placed at the bottom of the cell. The graphite substrate consisted of 4 graphene layers and contained 10,320C atoms. A constant electric field of 10^4 V / m, which propelled silicon ions to the graphite substrate, was applied to the cell. A Si^{4+} ion was launched from the top of the cell every 30 ps. During this time period the Si^{4+} ion managed to overcome the entire electrolyte filling of the cell and to find the appropriate place on the graphite substrate, where a single-layer film of pure silicon was formed. The Si^{4+} ion lifetime was 30 ps. The rest of the time, Si^{4+} ions existed in the form of neutral atoms. A Si^{4+} ion transform into a neutral atom, when it receives four electrons from the cathode, i. e. the graphite substrate. The interaction of Si^{4+} ion in molten salt was described by the Lennard-Jones (LJ) potential with the Coulomb term and the interaction between silicon and melt components as well as the interaction of silicon or salt melt with a graphite substrate were represented by the LJ

potential [33]. The cutoff radius for pairwise potentials was $r_{cut} = 8$ Å. The Si-Si and C—C interactions was represented using the Tersoff potential [34]. At the final calculation stage, the single-layer silicon film was obtained, the calculation was performed in the NVT ensemble at $T = 1000$ K. The molecular dynamic (MD) method of silicon deposition on the graphite substrate and interfacial properties of the "KF-KCl-KI melt-silicon film" system are described in [33]. In the present work, we focused on describing the structure of the used electrolyte.

The mean square of the displacement (MSD) for ions of the k salt melt component is represented as follows:

$$\left\langle (\Delta r)^2 \right\rangle_k = \frac{1}{n}\sum_{j=1}^{n}\left\{\frac{1}{N_k}\sum_{i=1}^{N}\left[\boldsymbol{r}_{k,i}(t+t_0)-\boldsymbol{r}_{k,i}(t_0)\right]^2\right\} \quad (2)$$

where t is the observation time of the i ion displacement $\boldsymbol{r}_{k,i}(t+t_0)-\boldsymbol{r}_{k,i}(t_0)$, starting from some initial moment t_0, n is the number of initial times, N_k is the number of particles of type k.

The partial diffusion coefficients of ions were calculated according to the expression

$$D_k = \frac{1}{2\Gamma}\lim_{t\to\infty}\frac{1}{t}\left\langle (\Delta \boldsymbol{r})^2 \right\rangle_k \quad (3)$$

where for three-dimensional space $\Gamma = 3$, t is the observation time of the ion displacement.

To compare the average self-diffusion coefficient D of all ions, which was obtained by the molecular dynamics method, with the corresponding experimental characteristic, it is proposed to take into account the dependence of the self-diffusion coefficient on the size of the system. The Yeh – Hummer (YH) method [35] allows to perform this comparison within a shortest possible time. The estimation of the real self-diffusion coefficient is carried out in accordance with the formula:

$$D_\infty = D(L) + 2.837298\frac{k_B T}{6\pi\eta L} \quad (4)$$

where $D(L)$ is the self-diffusion coefficient calculated by the molecular dynamics method with the edge length of the main MD cell equal to L; k_B is the Boltzmann constant; T is the absolute temperature; η is the shear viscosity of the melt.

Partial distribution functions in the system were defined as

$$g_{\alpha\beta}(r) = \frac{V n_\beta(r)}{4\pi N_\beta r_{\alpha\beta}^2} \quad (5)$$

where V is the volume of the simulation box, $n_\beta(r)$ is the number of particles of species β located distance r from a given particle of species α, N_β is the number of particles of species β, and $r_{\alpha\beta}$ is the distance between particles α and β.

Radial distribution functions are determined by the Fourier transformation from the experimentally determined structural factors or calculated directly using the appropriate models. Partial structural factors can be determined by various methods, including neutron diffraction and isotope substitution [36–38]. Due to a large number of technical obstacles the reliable reproducible experimental data for the structure of molten salts can be hardly obtained [39].

Partial structural factors $S_{\alpha\beta}(k)$ were calculated according to the formula:

$$S_{\alpha\beta}(k) = 1 + \frac{4\pi N}{kV}\int_0^\infty \left(g_{\alpha\beta}(r)-1\right)\cdot r\cdot sin(kr)\mathrm{d}r \quad (6)$$

where V is the volume of the sample, N is the total number of ions in the sample, the function $g_{\alpha\beta}(r)$determines the distribution of β-ions observed from the α-ion.

The short-range order of atomic packing in a molten salt can be investigated in more detail than it is represented by the partial radial distribution functions. in the present study we carry out a detailed quantitative analysis of the mutual arrangement of neighbors within the first coordination sphere that is determined from the first minimum of the calculated partial radial distribution function. This analysis includes the identification of the average quantitative composition of the first-order neighbors, represented by K^+, F^-, Cl^- and I^- ions located around the ions of each type.

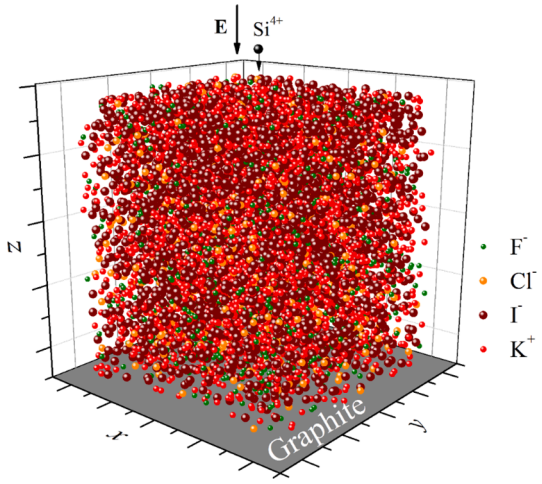

Fig. 1. Configuration of the KF-KCl-KI salt melt at 1000 K at the last stage of simulation (at the time 24 ns).

The radial distribution function, traditionally used to analyze the structure of condensed systems, represents the spherically symmetric arrangement of atoms around a selected center and has a single argument. The argument of this function is the distance from the center to the current sphere layer, where neighboring atoms can be located. Consequently, this function does not elucidate in detail of the local spatial structure of the studied environment. An accurate three-dimensional description of the local structure in the model can be obtained by Voronoi polyhedra (VP) and subsequent statistical analysis of the elements of these polyhedra [40–43]. A polyhedron is created around the selected center by drawing planes through and perpendicular to the midpoints of the line segments that connect the center to the intended nearest neighbors. The polyhedron allocates the territory for each selected center, so that all inner points of the polyhedron are closer to its center than to any other atomic center. Thus, using the construction of VP, an exhaustive idea of the nature of the nearest arrangement of atoms in a substance can be obtained. In particular, the number of VP faces reflects the number of the nearest geometric neighbors, and the number of the face sides shows the composition of an atomic cyclic formation, which is seen from the center of VP in a given direction. In a multicomponent system, it is possible to construct hybrid VPs, when the polyhedron faces are formed by atoms different from the central atom. This makes it possible to determine the environment of atoms, creating by any other atoms. Such analysis can be supplemented by the construction of partial radial distribution functions.

The open-source LAMMPS code for parallel computing in the MD method was used [44]. All calculations were performed using a URAN cluster-type hybrid computer at the IMM UB RAS with a peak performance of 216 Tflop/s and 1864 CPU.

3. Results and discussion

Fig. 1 shows the KF-KCl-KI salt melt at the last stage of simulation (at the time 24 ns). As can be seen from Fig. 1, a high level of mixing of the molten salt has been achieved. However, due to the high concentration of K^+ and I^- ions, small groups formed by these ions can be observed.

We carried out one more additional comparative study of the structure of a silicon film obtained by the electrodeposition in the MD model. The electrodeposition of silicon carried out for 24 ns led to the formation of a thin Si film, its structural relaxation was performed in the absence of the melt by the MD calculation for 2 ns at a temperature of

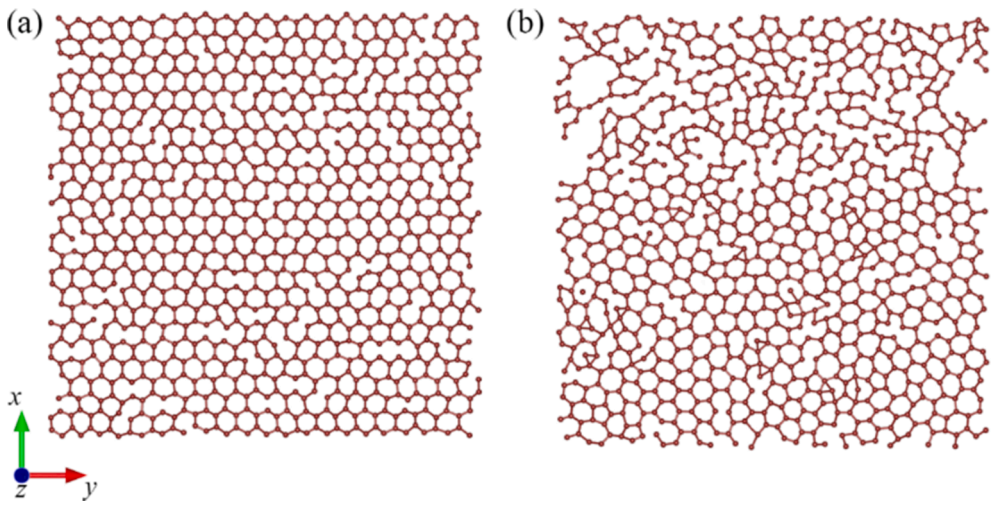

Fig. 2. *Xy* - projections of two-dimensional silicon located on a graphite substrate at a temperature of $T = 1000$ K; (a) - single-layer silicene (b) - deposited silicon film; calculations were performed by MD simulation; the positions of Si atoms in both configurations are averaged over a time interval of 1 ns. The deposited film contains a small number of Si atoms belonging to the second layer. The arrows show the direction of the coordinate axes.

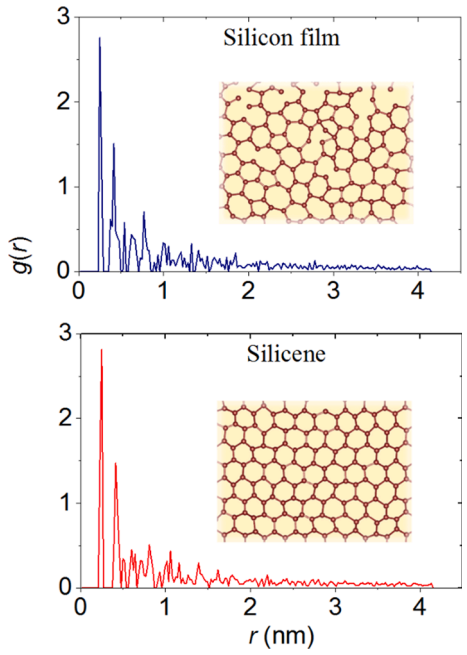

Fig. 3. Radial distribution functions obtained for a silicon film deposited on graphite and for silicene lying on graphite at $T = 1000$ K. The insets show fragments of objects corresponding to these functions.

1000 K. The film has a predominantly cellular hexagonal structure (Fig. 2b). For comparison, Fig. 2a shows the configuration of silicene on a graphite substrate of the identical size, obtained by the MD calculation over a time interval of 2 ns at the same temperature (1000 K). The silicene structure is formed by 1008Si atoms, while the deposited silicon film is represented by 982Si atoms. Some Si atoms in the film are located above the others; these atoms begin to form the second layer, although the first layer of the film is not fully formed yet (Fig. 2b). The *xy*-projections of silicon film and silicene were built using the VESTA program [45]. The bond between Si atoms was not detected in the cases when within 2 ns the distance between the atoms changed by more than 0.02 nm, i.e. by about half buckling (0.044 nm) in free-standing silicene. The radial distribution functions $g(r)$ calculated for one Si atom closest to the center of the sheet in a time interval of 2 ns are shown in Fig. 3 together

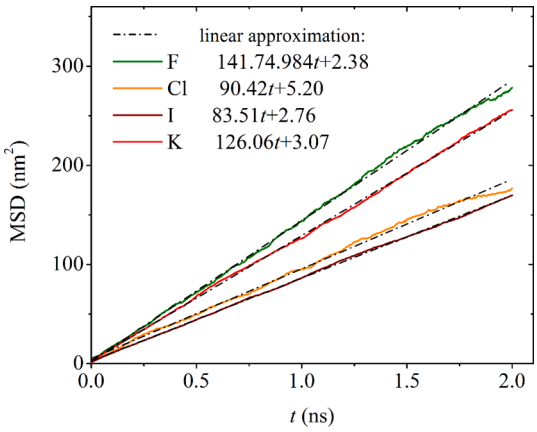

Fig. 4. Time dependence of the mean square displacement of F^-, Cl^-, I^-, and K^+ ions in the KF-KCl-KI salt melt at 1000 K and linear approximation of this dependence. The time is counted from the moment of the start of the main calculation.

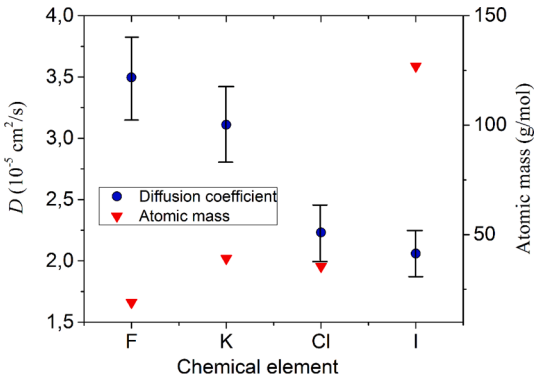

Fig. 5. Diffusion coefficients of F^-, Cl^-, I^-, and K^+ ions in the KF-KCl-KI salt melt at a temperature of 1000 K and the atomic masses of the corresponding chemical elements. The bars denote estimated errors associated with the determination of self-diffusion coefficient in a system with a limited number of ions.

with small fragments of the objects they describe. The calculated

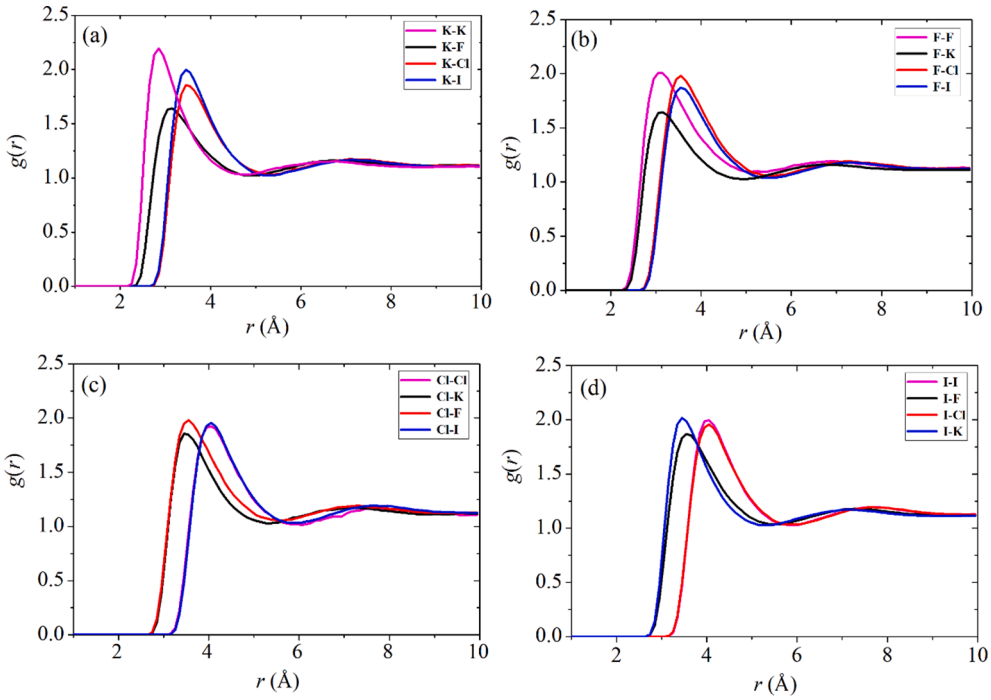

Fig. 6. Partial radial distribution functions of the KF-KCl-KI melt at a temperature of 1000 K. The first chemical element in the legend indicates the ion, around which *g* (*r*) is constructed. The neighbors considered for this ion are determined by the second element in each pair.

functions *g*(*r*) have a similar shape, reflecting the closeness of the two-dimensional structures under consideration. However, for silicene, a sharper second peak of the function *g*(*r*) is observed, which reflects a more ordered arrangement of the second neighbors. In other words, the silicene structure turns out to be more ordered.

The time dependence of the salt melt ions mean square displacement is shown in Fig. 4. Each dependence $< \Delta r^2 > (t)$ was obtained by averaging over 10 initial times t_0. A linear approximation of the corresponding calculated dependencies is also presented in the legend by analytical expressions. As can be seen from the figure, there is a high degree of agreement between the calculated dependences $< \Delta r^2 > (t)$ and their linear approximations.

The calculated diffusion coefficients of F^-, Cl^-, I^-, and K^+ ions in the KF-KCl-KI salt melt at a temperature of 1000 K are shown in Fig. 5. The atomic masses of the corresponding chemical elements are also shown here. It can be seen that, as a rule, the diffusion coefficients of elements are in the inverse ratio to their mass. Only for K^+ ions, which have a slightly larger mass than Cl^- ions, the diffusion coefficient is noticeably higher than for chlorine ions. Potassium ions, unlike chlorine ions, carry a positive electrical charge. They are accelerated when interacting with negatively charged I^- ions, which have a significantly greater mass. This is reflected in the value of the diffusion coefficient, since there are 2.47 times more heavy I^- ions in the system under study than the F^- and Cl^- lighter ions.

In the absence of experimental data on the diffusion coefficient for the KF-KCl-KI system, it makes sense to compare our calculated values of the coefficient *D* and those reported in [46], where ab initio MD simulation of the KF – NaF – AlF_3 system was performed at a temperature of 1100 K. The diffusion coefficient of fluorine ions in this system is in the vicinity of $4 \cdot 10^{-5}$ cm^2 / s, and the D value for potassium ions changes from $1.5 \cdot 10^{-5}$ to $5.5 \cdot 10^{-5}$ cm^2 / s with an increase in the KF concentration from 2 to 18 wt%. The values of the coefficients *D* obtained in this work for the F^- and K^+ ions are 3.49 $9 \cdot 10^{-5}$ and $3.11 \cdot 10^{-5}$ cm^2 / s, respectively.

Thus, the average self-diffusion coefficient in the model KF-KCl-KI melt is $D(L) = 2.72 \cdot 10^{-5}$ cm^2/s at the average value of the MD cell edge $L = 7.7$ nm. The experimental value of the shear viscosity for such a melt at a temperature of 984 K is 2.1 mPa·s [47]. Then the required correction for determining the coefficient D_∞ is $2.65 \cdot 10^{-6}$ cm^2/s, i.e. is approximately 9.7% of the $D(L)$ value. We accept this relative error (9.7%) for all values of the calculated partial self-diffusion coefficients. The molecular dynamics study of contact melting of the significantly smaller KCl-KI systems composed of only 216 ions using identical interatomic interaction potentials illustrated that, the average ion diffusion coefficient was equal to $2.78 \cdot 10^{-5}$ cm^2 / s at a temperature of 1000 K [48].

In general, the values of the diffusion coefficients of different types of ions are located in the sequence of their inverse atomic masses. Chlorine ions, which ionic radius is 1.31 times larger than that of K^+ ions having a ~ 12% greater atomic mass are the only exceptions in this sequence. The deceleration of Cl^- ions in the melt is facilitated by the large ionic radius. A joint decrease in the diffusion coefficient for ions of different types could occur if they formed associates. However, in the present study, we did not observe such phenomenon.

The ionic charge in a liquid electrolyte tends to overcome the influence of an external field [49]. This leads to structural changes in the electrolyte. Its structure differs from the structure of a free electrolyte without electric field. The interaction between the cations and anions forming the electrolyte is weakened in the presence of an electric field. It is equally important that the multiply charged cations (Si^{4+}) constantly present in the salt melt attract anions, i.e. they most often form single charged virtual clusters in a liquid electrolyte [50]. It also weakens the interaction between the major carriers of the positive and negative charge. The ongoing structural changes affect the form of the partial radial distribution functions, which for brevity will be denoted as g_{++} (cation-cation), g_{--} (anion-anion) and g_{+-} (cation–anion). As a result, the first peak of the partial radial distribution function g_{+-} or g_{-+} no longer falls on a shorter distance than that of the functions g_{++} or g_{--}, as in the case for simple two-component salt melts [30].

The calculated partial radial distribution functions of ions in the KF-KCl-KI melt are shown in Fig. 6. It can be seen that the partial functions *g* (*r*) constructed for each ion are split into pairs determined by the location of the first peak of this function. The displacement of the location of the first peak towards short distances is observed for the functions K-K, K-F; F-F, F-K; Cl-F, Cl-K; I-F, I-K. Among the ions considered here, F^-

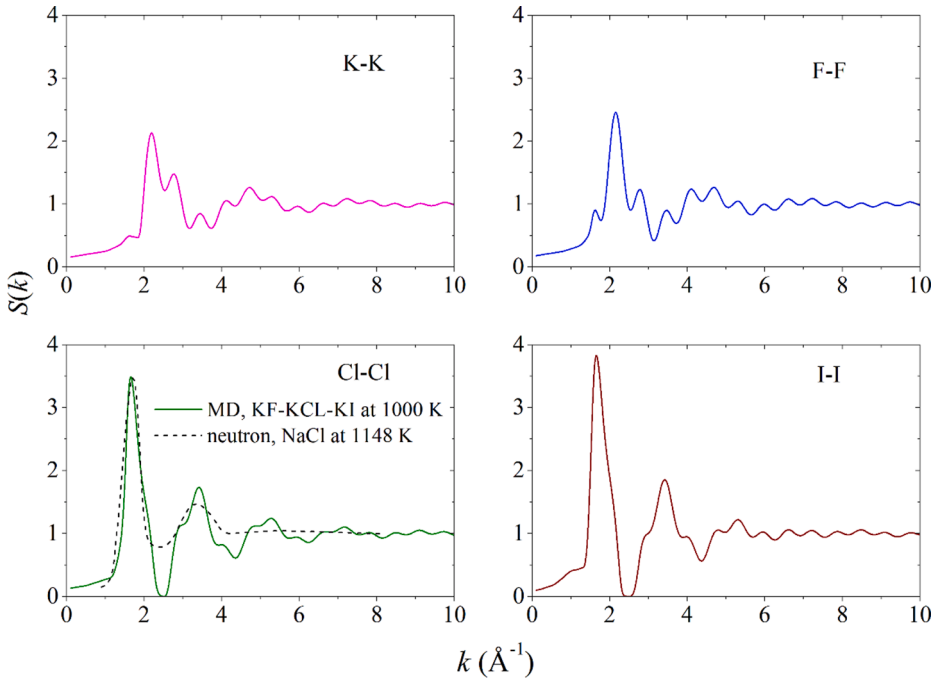

Fig. 7. Partial structural factors for the similar ions in the KF-KCl-KI salt melt at a temperature of 1000 K; neutron scattering data were obtained for NaCl melt at 1148 K [52].

(0.133 nm) and K^+ (0.138 nm) have the smallest radii, and Cl^- (0.181 nm) and I^- (0.220 nm) have the largest ones. The first peaks of the partial functions $g(r)$ turn out to be shifted to the left for ion pairs with the minimum sum of ionic radii. Thus, in the case when the K^+ ion is included in the ion pair, the first peaks of the K-K and K-F functions are shifted more to the left than the analogous peaks of other functions (Fig. 6a). However, despite the fact that the sum of the radii of the K-K ion pair is somewhat larger than the similar sum of the K-F pair, the main peak of the K-K function is located to the left. This is due to the fact that the number of K^+ ions in the system is 5.2 times greater than the number

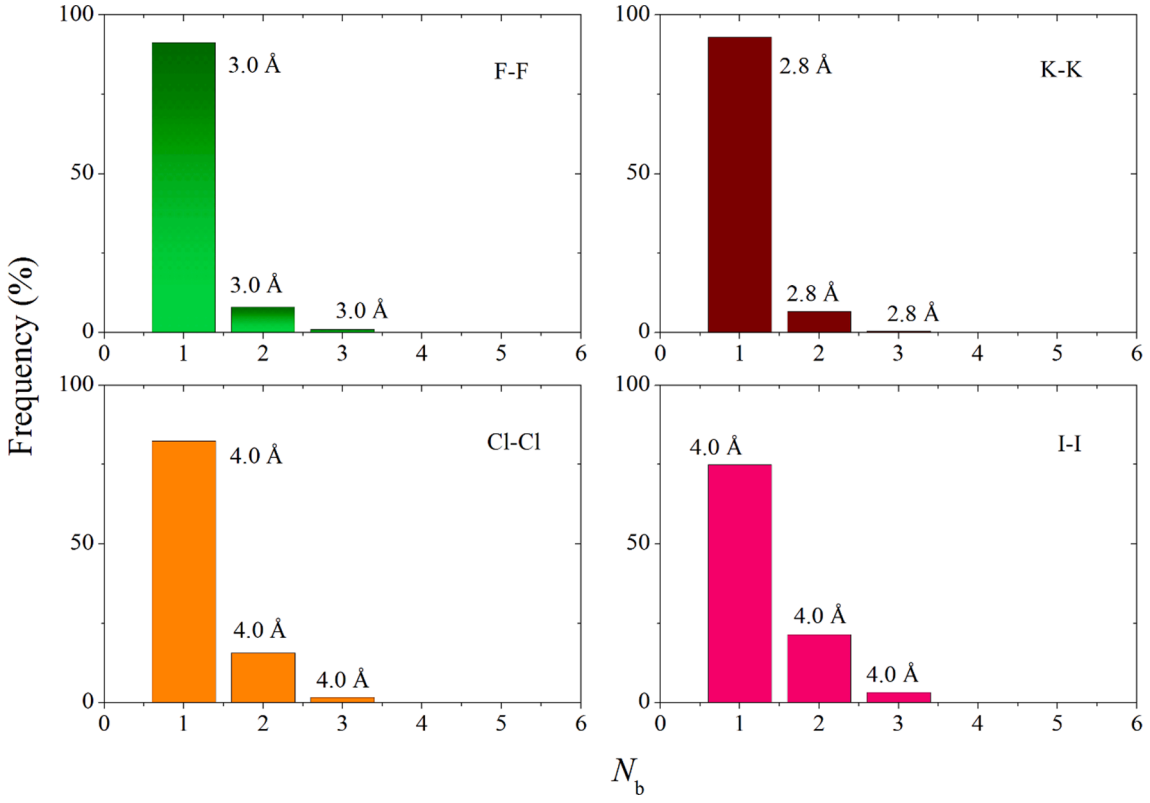

Fig. 8. Frequency of the appearance of single, double and triple contacts between similar ions in the KF-KCl-KI salt melt at $T = 1000$ K; the corresponding average lengths of associations are also indicated.

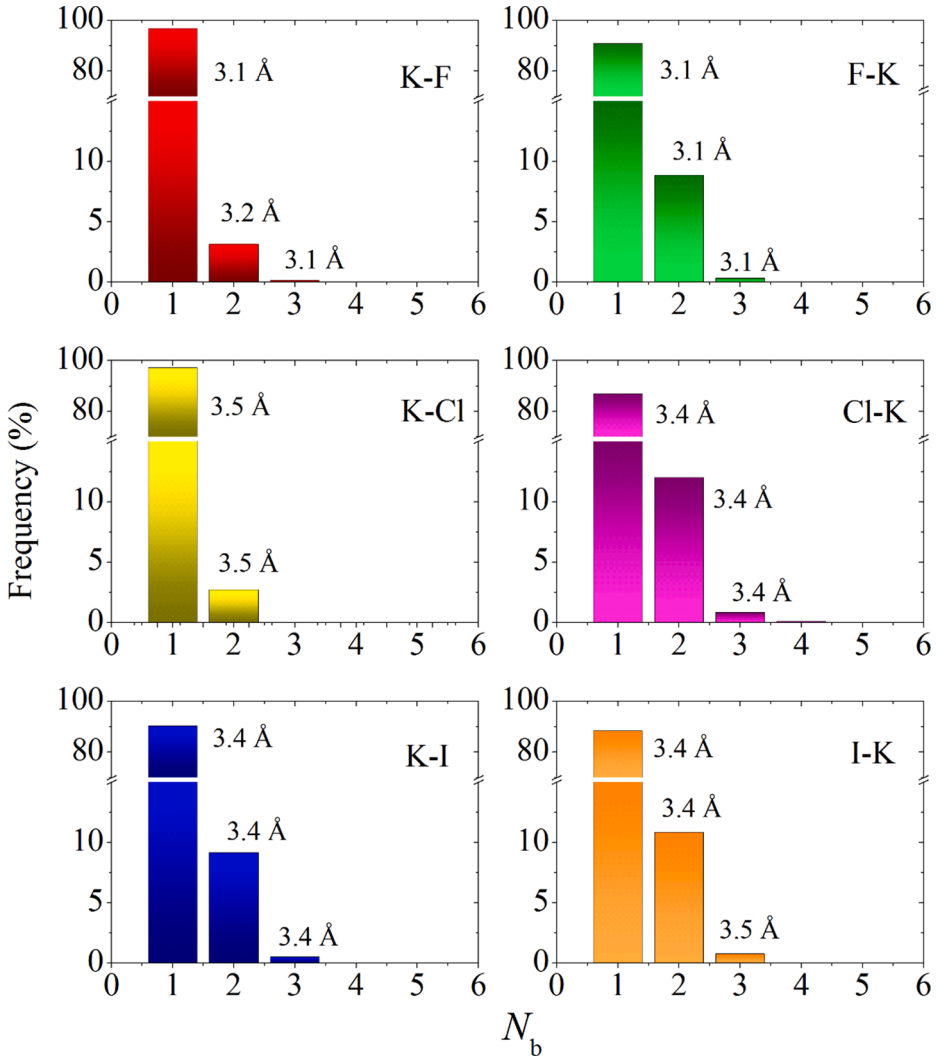

Fig. 9. Frequency of the appearance of single, double and triple contacts between halogen ions and potassium ions in the KF-KCl-KI salt melt at $T = 1000$ K; the corresponding average lengths of associations are also indicated.

of F^- ions.

The radial distribution functions calculated using the Born-Mayer-Huggins potential have rather gentle slopes of the first maximum. This is indicative of the soft core created by this potential. The presence of a soft core contributes to the rapid decay of the structural factor [51]. The calculated partial structural factors characterizing the structure and stability of subsystems of like ions are shown in Fig. 7. The influence of small-scale thermal fluctuations on the shape of these functions was not eliminated for a more adequate comparison of these characteristics. Therefore, small fluctuations are present in the $S(k)$ dependences, especially in the "tail" of these functions. Oscillations in the used interaction potential have a greater effect on the intensity of the first peak of the function $S(k)$ than on its shape at large values of k [52]. We compared the structure factor of the Cl-Cl subsystem with the corresponding function obtained by neutron scattering using the liquid NaCl molten salt at a temperature of 1148 K. The intensities and locations of the first and, partly, the second peak of the function $S(k)$ for these liquid systems coincide well. At the same time, the peaks of the $S_{\text{Cl-Cl}}(k)$ function obtained for the KF-KCl-KI salt melt are resolved much more strongly than the peaks in the NaCl melt. This is obviously due to the presence of three "foreign" components (K, F, I) in the ternary melt, and in a binary melt there is only one such component (Na). The appearance of the third and more distant peaks of the partial function $S(k)$ is facilitated not only by an increase in the mass of the ions under consideration, but also by their lower concentration in the salt melt, which can be seen from the comparison of $S(k)$ for subsystems formed by halogens.

In the salt melt under study, all ions have the same electric charge in absolute value. In such melt, the dynamic properties of ions are mainly determined by their atomic mass. Using average distances that are realized in the first coordination sphere that is assigned to each of the calculated partial radial distribution functions, we determined the number of the nearest neighbors of each sort near the selected center (ion). Rapid mixing of ions occurs in the high temperature salt melt; therefore, all determined groups of ions are unstable and disintegrate rapidly.

Ions in a molten salt can come into contact with similar ions one time or repeatedly. Among multiple contacts, only double and triple contacts are quite noticeable. The frequency of occurrence of single, double, and triple contacts (N_b distribution) of similar ions in the KF-KCl-KI salt melt at a temperature of 1000 K is shown in Fig. 8. The average lengths of associations corresponding to each number of contacts are also shown. The largest deviation (2.76%) of the length of association from the corresponding characteristic obtained in the presence of a single contact is observed in the case of the formation of triple F-F contacts, and the smallest (0.07%) - in the case of formation of triple K-K contacts. As can be seen from Fig. 8, single contacts dominate in all cases of neighboring similar ions, and their proportion ranges from 74 to 93%, double

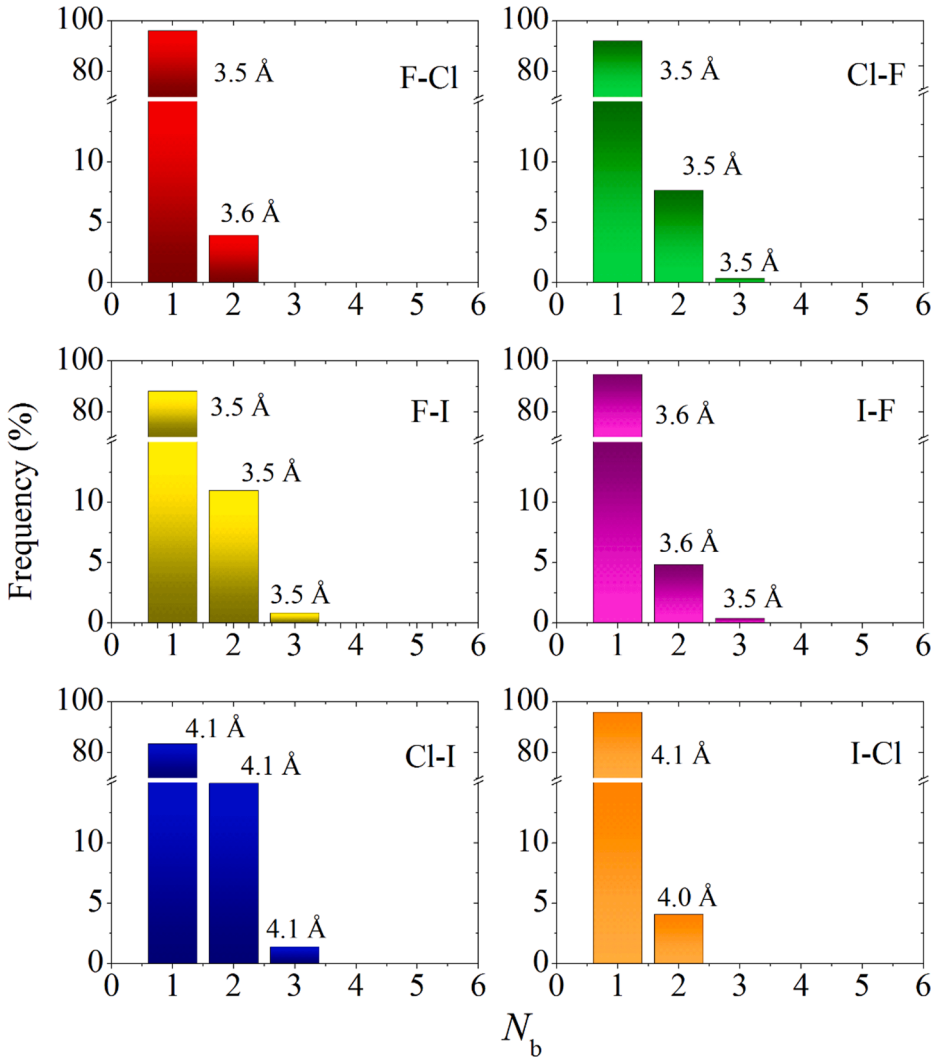

Fig. 10. Frequency of the appearance of single, double and triple contacts between halogen ions in the KF-KCl-KI salt melt at $T = 1000$ K; the corresponding average lengths of associations are also indicated.

contacts appear in 6–21% of cases, and the proportion of triple contacts does not exceed 3.3% (for I-I local packings). The heavier ions were found to have the greater number of double and triple contacts with similar ions.

The contact pattern of different types of ions is generally similar to the contact pattern of similar ions (Fig. 9). Single contacts also prevail here (83–97%). The proportion of double contacts ranges from ~ 3 to 12%, and the number of triple contacts is very insignificant (up to 1%). Note that, in this case, there is a significant asymmetry with respect to the change in the role of ions in the formation of the first coordination sphere, i.e. N_b distributions are unequal with respect to the permutation of the symbols denoting them. In other words, when two types of ions (A and B) are considered, the N_b distributions defined as A-B can differ significantly from the corresponding distributions B-A. Obviously, this is due to the influence of ions of other types on the formation of packing of any selected charged particles of two different types.

The number of double contacts increases when heavy halogen ions are arranged around lighter halogen ions, as is the case with the F-I and Cl-I packings (Fig. 10). When placing the opposite type, i.e. I-F and I-Cl the number of double contacts is reduced by 2–3 times. However, this is most likely associated not with the mass of ions, but with their amount in the salt melt. So the number of pairs of lighter ions F^- located around the Cl^- ion is 2 times larger than the number of pairs of heavier Cl^- ions located around the F^- ions. Recall that the number of F^- ions in the melt is 2 times higher than the number of Cl^- ions, and the number of I^- ions is much higher (2.47 times) than the number of F^- and Cl^- ions taken together.

The Voronoi polyhedra determine the number of neighbors among the atoms of the same kind as the central atom in the construction. The distributions of such polyhedra by the number of faces (neighbors of the same type) are shown in Fig. 11. As can be seen from Fig. 11, the distributions of VPs over the number of faces (n distribution) are rather uniform for the subsystems formed by lighter ions (K^+, F^-, Cl^-). In these cases, the maximum n distribution falls on $n^* = 14$, and the shape of the distributions is close to symmetric. At the same time, for the subsystem of the heaviest ions (I^-), the n distribution is clearly asymmetric, and its maximum fall on $n^* = 17$. This form of the calculated n distributions is mainly determined by the dynamic properties of the ions.

Distributions by the number of sides (m distributions) in faces for the same type of Voronoi polyhedra, built for the subsystems formed by similar ions, turn out to be in many respects similar (Fig. 12). The range of significant values of m in these distributions is bounded on the right by the value $m_{max} = 10$, and the maximum of the distribution fall on the value $m^* = 5$. The last circumstance means that rotational symmetry of the fifth order, which is characteristic of the structure of a simple liquid, prevails in the in most of the structure of similar atoms in the studied melt [52–55].

The angular distribution (θ distribution) of the same type of

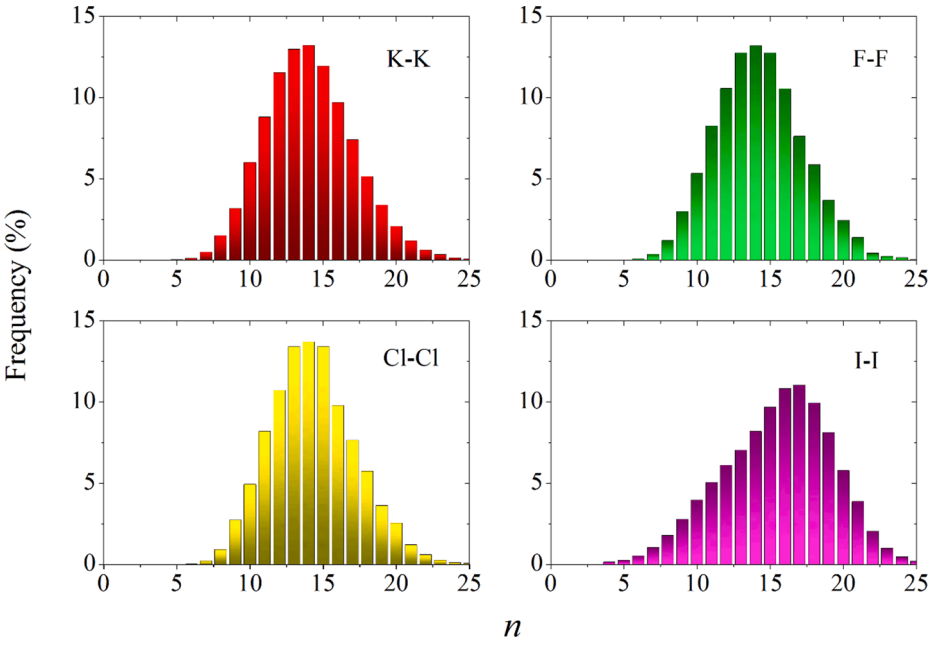

Fig. 11. Distribution of similar Voronoi polyhedra by the number of faces.

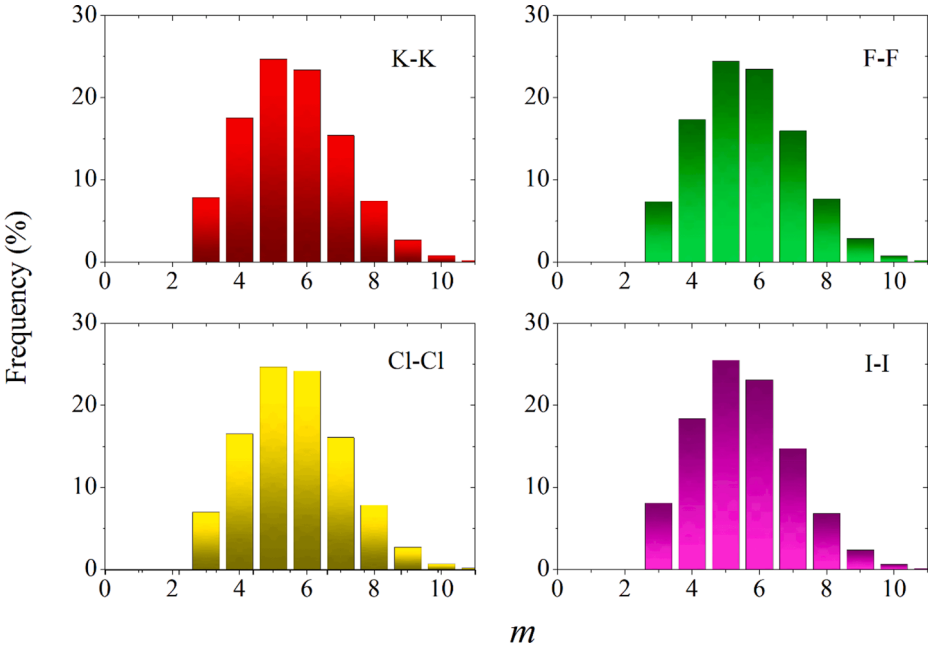

Fig. 12. Distribution of Voronoi polyhedra faces built for similar ions, by the number of sides.

geometric neighbors for all considered ion pairs (Cl-Cl, F-F, K-K, and I-I) has a form characteristic of the θ distribution of disordered mixtures formed by atoms of different sizes (Fig. 13) [43]. The angles θ considered here are formed by the pairs of ions giving the VP faces and by the center of the polyhedron (the vertex of the angle) in which the selected ion is located. The θ distribution reaches a maximum at angles of 93° for the distributions formed by K^+, F^-, Cl^- ions, and 84° for the distribution derived from the placement of I^- ions, respectively. A feature of all obtained θ distributions is the extremely small number of cases when the angle $\theta = 0°$ or 180°, i.e. when the centers of the three ions forming this angle lie on one straight line. Examples of additional structural characteristics calculated based on consideration of various ion pairs are presented in Supplementary Material.

In the experimental electrodeposition of a silicon film, 0.5 mol% K_2SiF_6 was introduced into the KF-KCl-KI melt [20]. As a result of the decomposition of this component, KF and SiF_4 were formed. SiF_4 is in gaseous form and at a temperature of 1033 K it intensively evaporates from the melt [56]. KF decays into ions K^+ and F^-. The presence of fluorine ions in the molten salt is necessary for the growth of a silicon film on the cathode. The products of the primary reaction between F and Si in the melt are SiF radicals, which passivate the cathode surface when deposited on the cathode. The second reaction:

$$2SiF(a) \xrightarrow{SV}_{DB} SiF_2(a) + Si(s) \quad (7)$$

results in the formation of SiF_2 molecules and their desorption, while Si atoms remain at the cathode surface [57]. In the reaction equation (7),

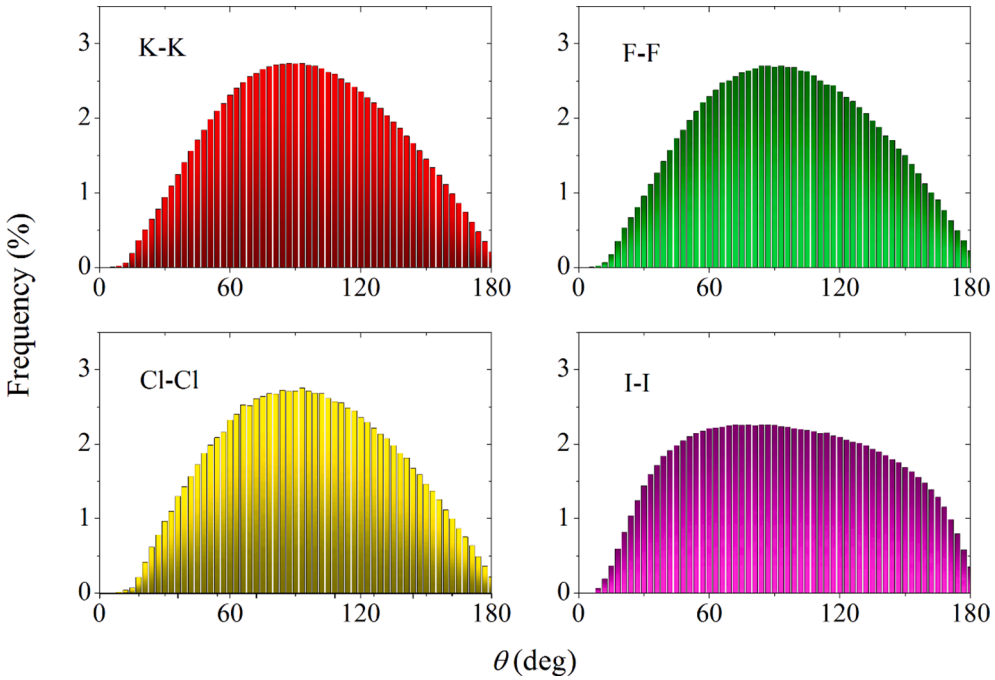

Fig. 13. Angular distribution of similar geometrical neighbors in the KF-KCl-KI salt melt at a temperature of 1000 K.

the following designations are accepted: SV is the surface vacancy and DB is the dangling bond, (a) denotes adsorbed silicon, and (s) denotes solid silicon. The transformation of SiF radicals into SiF_2 molecules occurs in the presence of surface defects, which has been experimentally proven [58]. It was shown that at low temperatures in the gas phase, SiF_2 molecules are transformed into SiF_4 molecules [59]. Our calculations show that the variation of the composition of the molten salt influences the process of silicon deposition. So mobile light ions, such as K^+, will create uniformity in the distribution of SiF radicals in the melt, while the presence of a large number of heavy ions, such as I^-, will provoke a slowdown of these radicals before they are deposited on the substrate.

The SiF radical can be formed when the Si^{4+} ion passes through the KF-KCl-KI salt melt. The diffusion of ions in this melt ultimately determines the rate of Si film formation at the graphite surface according to reaction (7). Indeed, the $\dot{C}$ rate of change in the concentration of SiF radicals at the cathode (graphite) surface is given by the reaction–diffusion equation

$$\dot{C} = D \cdot C/\tau + r \tag{8}$$

where D is the average bulk diffusion coefficient of all ions, C is the local concentration of SiF radicals measured near the cathode, τ is the tortuosity that gives the effective diffusion length for the diffusion flow, r is the reaction density, so that in the absence of a reaction, $r = 0$.

Considering only one reaction (7) occurring at the cathode and using the empirical Butler – Volmer equation [60], the value of r can be determined as [61]

$$r = \sigma \cdot k_r C \cdot exp\left(\alpha \frac{e\phi}{k_B T}\right) \tag{9}$$

where σ is the cathode surface area density attainable for the reaction, k_r is the kinetic velocity associated with reaction (7), α is the charge transfer coefficient, e is the elementary electric charge, $\phi = \Phi - \Phi_0$ is the local potential relative to the average applied potential Φ_0,k_B is the Boltzmann constant, T is the absolute temperature. However, it is not possible to estimate the values of most of the parameters included in equations (8) and (9).

4. Conclusion

In this work, the kinetic properties are investigated and a detailed structural analysis of the KF-KCl-KI salt melt used for the electrolytic deposition of thin silicon films is performed. It is shown that the values of the diffusion coefficients of ions obey predominantly the inversely proportional dependence of their mass. Partial radial distribution functions constructed for each of the ions present in the melt are divided into two groups, which significantly differ in the location of the first maximum of this function. The atomic mass and the number of ions of a certain type in the salt melt have a significant effect on the structure of the short-range order of the melt. Heavy ions (I-) form a subsystem, which structure differs from the structure of subsystems of lighter ions (K^+, F^-, Cl^-). In particular, the heavy ion subsystem is characterized by the presence of asymmetry in the distributions of Voronoi polyhedra over the number of faces and in the angular distribution of the nearest geometric neighbors, which is not observed for subsystems of lighter ions. The difference in the sizes of the ions that make up the salt melt determines the specific domed shape of the angular distributions plotted for ions of the same type. All considered structural characteristics are important indicators of the physical properties of the molten salt intended for the deposition of high-purity silicon films. Guided by such characteristics, it is possible to select the optimal composition of the molten salt.

Thus, the molecular dynamics study of the kinetic properties and detailed structure of the molten salt can serve as an important tool in the selection of the appropriate composition of the salt, which is used in a heated form as a working fluid for obtaining ultrapure semiconductor films.

CRediT authorship contribution statement

Alexander Y. Galashev: Conceptualization, Methodology, Formal analysis, Visualization, Investigation, Writing – original draft, Writing – review & editing. **Ksenia A. Ivanichkina:** Visualization, Writing – review & editing.

Declaration of Competing Interest

The authors declare that they have no known competing financial interests or personal relationships that could have appeared to influence the work reported in this paper.

Acknowledgments

This work was carried out in the framework of agreement No. 075-03-2020-582 / 1 of 02/18/2020 (topic number 0836-2020-0037).

Appendix A. Supplementary material

Supplementary data to this article can be found online at https://doi.org/10.1016/j.chemphys.2022.111455.

References

[1] H. Kim, D.A. Boysen, J.M. Newhouse, B.L. Spatocco, B. Chung, P.J. Burke, D. J. Bradwell, K. Jiang, A.A. Tomaszowska, K. Wang, W. Wei, L.A. Ortiz, S.A. Barriga, S.M. Poizeau, D.R. Sadoway, Chem. Rev. 113 (2012) 2075.
[2] H. Li, H. Yin, K. Wang, S. Cheng, K. Jiang, D.R. Sadoway, Adv. Energy Mater. 6 (2016) 1600483.
[3] P. Masset, A. Henry, J.-Y. Poinso, J.-C. Poignet, J. Power Sources 160 (2006) 752.
[4] K.R. Harris, J. Phys. Chem. B 123 (2019) 7014.
[5] M. Gouverneur, F. Schmidt, M. Schönhoff, Phys. Chem. Chem. Phys. 20 (2018) 7470.
[6] A.E. Gheribi, K. Machado, D. Zanghi, C. Bessada, M. Salanne, P. Chartrand, Electrochim. Acta 274 (2018) 266.
[7] M.-M. Walz, D. van der Spoel, J. Phys. Chem. C 123 (2019) 25596.
[8] M.-M. Walz, D. van der Spoel, Phys. Chem. Chem. Phys. 21 (2019) 8516.
[9] A.T. Clay, C.M. Kuntz, K.E. Johnson, A.L. East, J. Chem. Phys. 136 (2012), 124504.
[10] N.P. Aravindakshan, C.M. Kuntz, K.E. Gemmell, K.E. Johnson, A.L. East, J. Chem. Phys. 145 (2016), 094504.
[11] N.P. Aravindakshan, K.E. Johnson, A.L. East, J. Chem. Phys. 151 (2019), 034507.
[12] L. Grantham, S. Yosim, J. Chem. Phys. 45 (1966) 1192.
[13] P. Masset, R.A. Guidotti, J. Power Sources 164 (2007) 397.
[14] K. Cornwell, J. Phys. D.: Appl. Phys. 4 (1971) 441.
[15] J. McDonald, H.T. Davis, Phys. Chem. Liq. 2 (1971) 119.
[16] A. Redkin, E. Nikolaeva, A. Dedyukhin, Y.u. Zaikov, Ionics 18 (2012) 255.
[17] A. Redkin, Y.u. Zaikov, O. Tkacheva, S. Kumkov, Ionics 22 (2016) 143.
[18] , A. Isakov, A. Kataev, A.A. Red'kin, Yu.P. Zaikov, Rus. Metallurgy 8 (2020) 918.
[19] , A. Isakov, , Yu.P. Zaikov, Rus. Metallurgy 9 (2019) 830.
[20] A. Isakov, , , Yu.P. Zaikov, J. Rheol. 65 (2021) 171.
[21] M.V. Laptev, A.V. Isakov, O.V. Grishenkova, A.S. Vorob'ev, A.O. Khudorozhkova, L.A. Akashev, Yu.P. Zaikov, J. Electrochem. Soc. 167 (2020) 042506.
[22] K. Yasuda, K. Maeda, T. Nohira, R. Hagiwara, T. Homma, J. Electrochem. Soc. 163 (2016) D95.
[23] K. Maeda, K. Yasuda, T. Nohira, R. Hagiwara, T. Homma, J. Electrochem. Soc. 162 (2015) D444.
[24] M.J.L. Sangster, M. Dixon, Adv. Phys. 25 (1976) 247.
[25] J. Wu, J. Wang, H. Ni, G. Lu, J. Yu, Appl. Sci. 8 (2018) 1874.
[26] Y. Wang, J. Shao, X. Zhu, Comp. Theor. Chem. 983 (2012) (2012) 38.
[27] Y. Laudernet, T. Cartailler, P. Turq, M. Ferrario, J. Phys. Chem. B 107 (2003) (2003) 2354.
[28] D. Zakiryanov, Non-empirical Calculations of Melting Temperatures, Thermal Conductivity Coefficients and Local Structure of Halogenide and Oxyhalogenide Melts. *Dissertation for a scientific degree candidate of chemical sciences.* (2021) 150 pp. Yekaterinburg. Institute of High-Temperature Electrochemistry, Ural Branch of the Russian Academy of Sciences.
[29] A. Baranyai, J. Mol. Liq. 297 (2020), 111762.
[30] H. Wang, R.S. DeFever, Y. Zhang, F. Wu, S. Roy, V.S. Bryantsev, C.J. Margulis, E. J. Maginn, J. Chem. Phys. 153 (2020), 214502.
[31] B.A. Frandsen, S.D. Nickerson, A.D. Clark, A. Solano, R. Baral, J. Williams, J. Neuefeind, M. Memmott, J. Nucl. Mater. 537 (2020), 152219.
[32] G. Bussi, T. Zykova-Timan, M. Parrinello, J. Chem. Phys. 130 (2009), 074101.
[33] K.A. Ivanichkina, A.Y. Galashev, A.V. Isakov, Applied, Surf. Sci. 564 (2021).
[34] J. Tersoff, Phys. Rev. B: Condens. Matter Mater. Phys. 39 (1989) 5566.
[35] I.-C. Yeh, G. Hummer, J. Phys. Chem. B 108 (2004) 15873.
[36] M.A. Howe, R.L. McGreevy, Phil. Mag. B 58 (1988) 485.
[37] R.L. McGreevy, M.A. Howe, J. Phys.: Condens. Matter. 1 (1989) 9957.
[38] M. Saito, S. Kang, Y. Waseda, Jpn. J. Appl. Phys. 38 (1999) 596.
[39] S. Sharma, A.S. Ivanov, C.J. Margulis, J. Phys. Chem. B 125 (2021) 6359.
[40] J.L. Finney, J. Comput. Phys. 32 (1979) 137.
[41] A.E. Galashev, V.P. Skripov, J. Struct. Chem. 25 (1984) 734.
[42] A.E. Galashev, V.P. Skripov, J. Struct. Chem. 26 (1985) 716.
[43] A.E. Galashev, V.P. Skripov, J. Struct. Chem. 27 (1986) 407.
[44] S. Plimpton, J. Comp. Phys. 117 (1995) 1.
[45] K. Momma, F. Izumi, J. Appl. Cryst. 44 (2011) 1272.
[46] X. Lv, Z. Han, H. Zhang, Q. Liu, J. Chen, L. Jiang, PCCP 21 (2019) 7474.
[47] A. Isakov, A. Khudorozhkova, A. Redkin, Y.u. Zaikov, J. Rheology 65 (2021) 171.
[48] V.S. Znamenskii, P.F. Zil'berman, P.A. Savintsev, E.A. Goncharenko, Inorganic Mater. 32 (1996) 536.
[49] J. Tong, S. Wu, N. vonSolms, X. Liang, F. Huo, Q. Zhou, H. He, S. Zhang, Front. Chem. 7 (2020) 945.
[50] K. Vékey, Mass Spectrometry Review 14 (1995) 195.
[51] C.A. Croxton, Liquid state physics: A statistical mechanical introduction, Cambridge University Press, London, 1974.
[52] F.G. Edwards, J.E. Enderby, R.A. Rowe, D.I. Page, J. Phys. C: Solid State Phys. 8 (1975) 3483.
[53] A.E. Galashev, Rus. J. Phys. Chem. B 8 (2014) 793.
[54] A.E. Galashev, Colloid J. 76 (2014) 300.
[55] A.N. Novruzov, O.R. Rakhmanova, A.E. Galashev, J. Struct. Chem. 70 (2008) 64.
[56] A.S. Vorob'ev, A.V. Isakov, A.Y. Galashev, Yu.P. Zaikov, J. Serb. Chem. Soc. 84 (2019) 1129.
[57] R. Knizikevicius, Sci. Rep. 10 (2020) 13634.
[58] K.S. Nakayama, J.H. Weaver, Phys. Rev. Lett. 83 (1999) 3210.
[59] P.L. Timms, R.A. Kent, T.C. Ehlert, J.L. Margrave, J. Am. Chem. Soc. 87 (1965) 2824.
[60] R.E. Jones, F.S. Gittleson, J.A. Templeton, D.K. Ward, J. Electrochem. Soc. 164 (2017) A6422.
[61] E.J.F. Dickinson, A.J. Wain, J. Electroanal. Chem. 872 (2020), 114145.